Foraging mechanisms in excavate flagellates shed light on the functional ecology of early eukaryotes

Suzuki-Tellier, Sei; Miano, Federica; Asadzadeh, Seyed Saeed; Simpson, Alastair G. B.; Kiørboe, Thomas

Published in:
Proceedings of the National Academy of Sciences of the United States of America

Link to article, DOI:
10.1073/pnas.2317264121

Publication date:
2024

Document Version
Publisher's PDF, also known as Version of record

PNAS RESEARCH ARTICLE | ECOLOGY

Foraging mechanisms in excavate flagellates shed light on the functional ecology of early eukaryotes

Sei Suzuki-Tellier[a,1], Federica Miano[a,1], Seyed Saeed Asadzadeh[a], Alastair G. B. Simpson[b], and Thomas Kiørboe[a,2]

Edited by David Karl, University of Hawaii at Manoa, Honolulu, HI; received October 6, 2023; accepted April 25, 2024

The phagotrophic flagellates described as "typical excavates" have been hypothesized to be morphologically similar to the Last Eukaryotic Common Ancestor and understanding the functional ecology of excavates may therefore help shed light on the ecology of these early eukaryotes. Typical excavates are characterized by a posterior flagellum equipped with a vane that beats in a ventral groove. Here, we combined flow visualization and observations of prey capture in representatives of the three clades of excavates with computational fluid dynamic modeling, to understand the functional significance of this cell architecture. We record substantial differences amongst species in the orientation of the vane and the beat plane of the posterior flagellum. Clearance rate magnitudes estimated from flow visualization and modeling are both like that of other similarly sized flagellates. The interaction between a vaned flagellum beating in a confinement is modeled to produce a very efficient feeding current at low energy costs, irrespective of the beat plane and vane orientation and of all other morphological variations. Given this predicted uniformity of function, we suggest that the foraging systems of typical excavates studied here may be good proxies to understand those potentially used by our distant ancestors more than 1 billion years ago.

early eukaryotic evolution | feeding current | prey capture | vane-bearing flagella | clearance rate

Significance

Human sperm reminds us of our ancestry: flagellates, unicellular organisms equipped with a flagellum. The last eukaryotic common ancestor (LECA) was a flagellate. Phylogenetic analyses suggest that excavates, an assemblage of flagellates, are the living organisms most similar to LECA. They have distinct characteristics in common: a ventral groove within which a vaned flagellum is beating. We show how the shared morphology and foraging behavior among 3 excavate clades is fluid dynamically efficient. We provide the first physical understanding of a major category of microbial foragers that are present in diverse aquatic systems, sometimes at high abundance. Crucially, it also allows credible inferences of the feeding capabilities of our distant ancestors living more than a billion years ago.

Phagotrophic flagellates are the main consumers of bacteria and pico-phytoplankton in the ocean and thus play a key role in regulating pelagic and benthic microbial ecosystems (1). They are phylogenetically very diverse, with representatives in all the major branches of the eukaryotic tree of life (Fig. 1*A*), and thus central to the evolution of all eukaryotes (2). They are also functionally diverse, as the number of flagella, their wave patterns and kinematics, and whether their flagella are naked or equipped with hairs or vanes vary between groups (3). Many species can also photosynthesize, i.e., they are mixotrophic. This functional diversity may imply great variation in foraging efficiency, as quantified by clearance rates that vary by more than two orders of magnitude between flagellates of similar sizes (4).

The mechanisms of phagotrophic foraging have been examined in only a few groups of flagellates that are numerically abundant and ecologically important in the upper marine water column. In the small-scale world of flagellates where the Reynolds number (ratio of inertial to viscous forces) is low, viscosity impedes predator–prey contact, and generating a sufficient feeding current typically requires forces that are larger than what a single naked flagellum can produce (9). Thus, in the groups examined in detail, one finds that the flagellar apparatus has highly specialized adaptations for foraging. For example, Stramenopiles have one flagellum equipped with rigid hairs that increases the force production of the beating flagellum by a factor of 5 to 10 (10, 11), and choanoflagellates have their single flagellum equipped with a vane that allows it to pump water through their collar filter (12, 13). Dinoflagellates are equipped with a transverse flagellum embedded in a "sock" and run in a groove around the cell circumference (14), which allows a very powerful feeding current (9).

"Typical excavates" are an assemblage of morphologically similar phagotrophic flagellates (15) that differ in overall cell architecture from the groups listed above and that are particularly important for understanding deep eukaryote evolution (Fig. 1*A*). They occur in the water column mainly attached to marine snow particles and may be highly abundant in anoxic marine waters but are found also in sediments (7, 16–21). The best-known forms are biflagellated cells with a naked anterior flagellum, and a posterior flagellum that beats in a ventral groove and bears 1 to 3 broad vanes of unclear function (7, 15) (Fig. 1). Each vane is formed by an intraflagellar (paraxonemal) protein lamella that distends the flagellar membrane, quite unlike the fine extracellular filamentous vanes of choanoflagellates. Bacterial prey is collected and engulfed in the posterior end of the groove, but the prey concentration and foraging mechanisms are essentially unknown.

Typical excavates belong to three major phylogenetic groups; Discoba, Metamonada, and Malawimonadida. Recent studies confirm and extend the strong morphological

Author contributions: S.S.-T., F.M., S.S.A., A.G.B.S., and T.K. designed research; S.S., F.M., S.S.A., and A.G.B.S. performed research; S.S.A. contributed new reagents/analytic tools; S.S., F.M., and T.K. analyzed data; and S.S., F.M., S.S.A., A.G.B.S., and T.K. wrote the paper.

The authors declare no competing interest.

This article is a PNAS Direct Submission.

[1]S.S. and F.M. contributed equally to this work.

[2]To whom correspondence may be addressed. Email: tk@aqua.dtu.dk.

This article contains supporting information online at https://www.pnas.org/lookup/suppl/doi:10.1073/pnas.2317264121/-/DCSupplemental.

Published May 23, 2024.

similarities of typical excavates across these three groups (7, 22, 23). Yet, contemporary molecular phylogenetic analyses place excavates as two or three separate, but extremely deep-branching clades, in the tree of eukaryotes (5, 7, 24), and these clades lie on either side of the root of eukaryotes in most recent analyses that include prokaryotic outgroups (6, 8, 25) (Fig. 1*A*). These data together suggest that the Last Eukaryotic Common Ancestor (LECA) may well have resembled living typical excavates (6, 7). This hypothesis is the best-supported specific version of the widely held view that LECA was a small biflagellate with a conspicuous feeding groove (26). Understanding the mechanisms of swimming and foraging in groove-bearing flagellates, and typical excavates in particular, may therefore help us infer how LECA cells used their flagella to feed and swim in the ancient past.

Here, we examine the mechanisms and fluid dynamics of foraging in several species of typical excavates belonging to Discoba, Metamonada, and Malawimonadida. We use high-speed videomicroscopy to describe the beating of the flagella and capture of prey, particle tracking to visualize the feeding current and to estimate clearance rates, and computational fluid dynamics (CFD) to understand the functional significance of the characteristic morphological features of excavate cells.

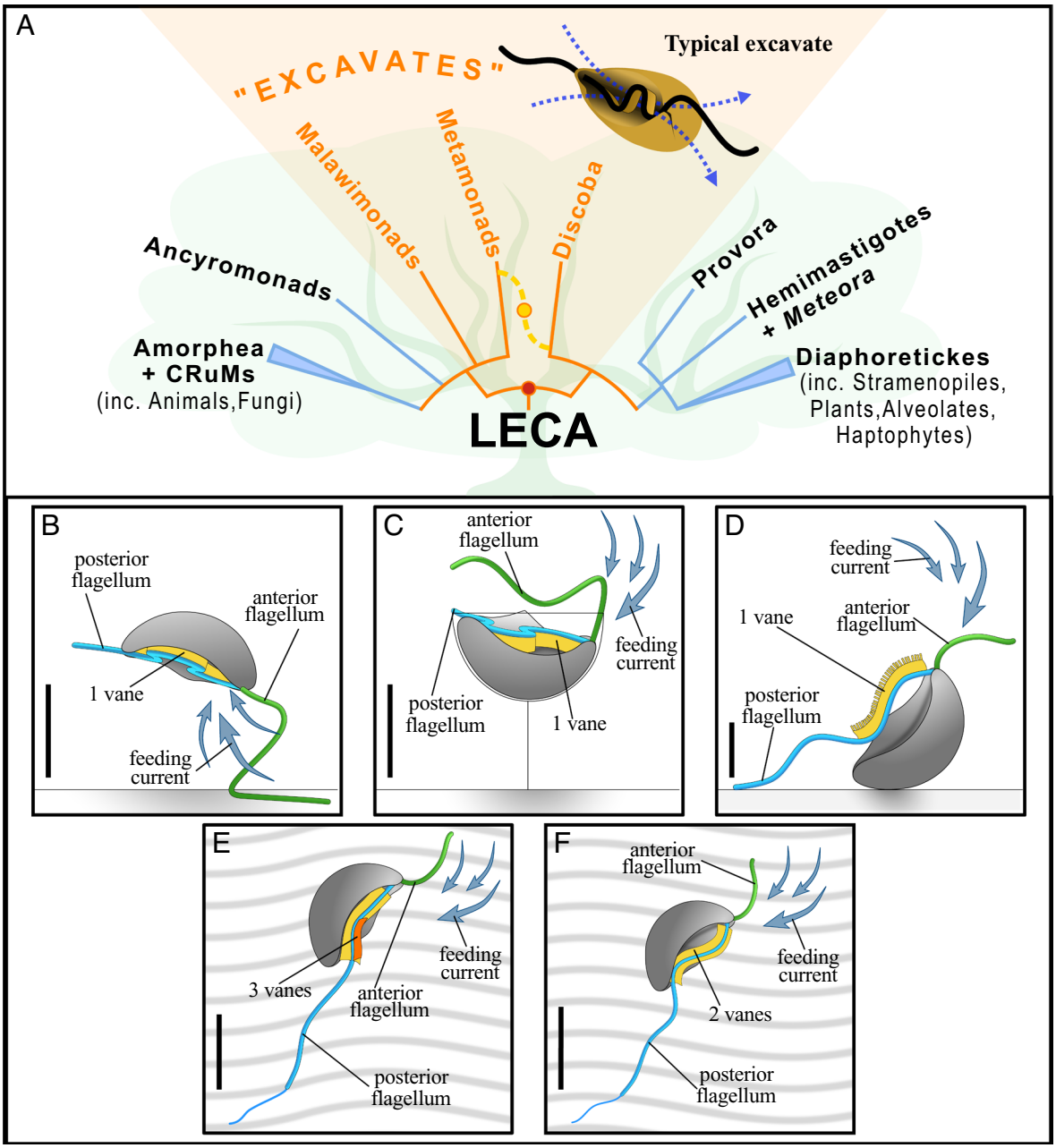

Fig. 1. (*A*) Summary tree of eukaryotes, showing current inferences that "excavates" represent extremely deeply branching lineages on either side of the root of eukaryotes, consistent with a common ancestry for the "typical excavate" cell architecture (orange) and an excavate-like LECA (red ball). Phylogeny after (5), with weakly supported branches collapsed and the two major clades containing most eukaryotes (Amorphea + CRuMs; Diaphoretickes) cartooned for clarity. The tree is rooted after (6). Some estimates of eukaryote phylogeny place Metamonada adjacent to Discoba [dashed yellow line; (7)], and one recent analysis suggests that the eukaryote root lies within metamonads [yellow ball; (8)]. These alternatives are also consistent with an excavate-like ancestry for all/virtually all extant eukaryotes. (*B–F*) Schematic representations of typical excavate species: (*B*) *Jakoba libera*, (*C*) *Reclinomonas americana*, (*D*) *Kipferlia bialata*, (*E*) *Carpediemonas membranifera*, and (*F*) *Malawimonas californiensis*. While foraging, *J. libera, R. americana,* and *K. bialata* are attached to the surface (bottom line); instead, *C. membranifera* and *M. californiensis* skid on the substrate (wavy background). Note that *C. membranifera* has a short third vane (orange). Reference scale bar, 5 μm.

Results

Feeding Behavior and Free-Swimming. Prey capture and handling follow a general pattern shared among all the species examined. The ventral groove extends for most of the length of the cell, with its right wall generally being taller and more continuous. A feeding current is generated by the flagella, always involving the posterior vane-bearing flagellum beating in the groove region with high amplitude waves at 25 to 50 Hz (Table 1). The behavior of the anterior flagellum differs among species.

The flow drives the prey into and through the ventral groove, entering roughly in the middle, and draws it toward the posterior end of the cell. Food particles are captured in the groove and handled near the phagocytosis site at its posterior end, where it is either phagocytized or rejected. Phagocytosis is facilitated by a moving "wave" of the cell membrane sweeping posteriorly along the groove, (Movies S2 and S3) (22). When the wave reaches the end of the groove, the particle is ingested with the membrane observed to affect the closure of the phagocytic vacuole.

When feeding, *Jakoba libera* attaches to a surface with a bent anterior flagellum (Fig. 1*B*). Often, the anterior flagellum will flex repeatedly and push the body backward and forward or change its orientation (Movie S1). The feeding current is generated by the posterior flagellum only. It extends a third of a body length outside of the cell, and this portion is straight and rigid. When swimming, the anterior flagellum is mainly responsible for propulsion as it beats in a three-dimensional power-and-return stroke while the posterior flagellum remains beating inside the groove (Movie S1).

In its feeding stage, *Reclinomonas americana* sits inside a lorica that is attached to the substrate with the ventral groove facing up (Movie S2) (Fig. 1*C*). It has a very tall and pronounced right wall. Uniquely, both flagella beat rapidly (Table 1). The anterior flagellum beats in a three-dimensional pattern above the ventral groove with the distal end pointing posteriorly. A short, straight portion of the posterior flagellum extends posteriorly beyond the groove and moves rigidly.

After cell division, one daughter cell remains in the parental lorica, while the other is free-swimming (17, 27). This swarmer is slender and highly mobile (Table 1) (Movie S2). Its anterior flagellum performs broader power-and-return strokes in front of the cell with the distal tip always pointing posteriorly. The posterior flagellum is longer (approximately 2 body lengths) and trails freely, beating along the groove.

Kipferlia bialata attaches to a surface with the posterior end of the cell body, normally with the groove facing away from the surface and generating a feeding current with both flagella (Movie S3) (Fig. 1*D*). The anterior flagellum performs slow (<10 Hz) three-dimensional power-and-return strokes. The posterior flagellum also beats in 3 dimensions but much faster (~30 Hz). When free-swimming, the flagellar kinematics remain the same. The anterior flagellum is responsible for displacement and causes the cell body to rotate on its longitudinal axis (Movie S3).

Carpediemonas membranifera and *Malawimonas californiensis* have similar feeding behavior and flagellar kinematics (Movie S4) (Fig. 1 *E* and *F*). When feeding, the cell attaches to surfaces with the distal quarter of the posterior flagellum and the cell hovers or skids around while generating a feeding current with both flagella. The anterior flagellum executes slow power-and-return strokes similar to *K. bialata*. The posterior flagellum beats only with the portion that is inside the groove. *C. membranifera* does not rely solely on feeding currents to capture prey, being recorded as "scooping" inside the groove a particle that was attached to the surface through movement of the cell body (Movie S4). Swimming cells use the posterior flagellum for propulsion (Movie S4). The overall contribution of the anterior flagellum to motility is minor and possibly more dedicated steering.

The Ventral Groove and the Flagellar Vane. The portion of the posterior flagellum inside the groove is equipped with vanes making much of the flagellum itself paddle-shaped. These thin extensions of the flagellum double, at least, its surface area and are somewhat flexible. We observed the number of vanes, their orientation, and their spatial-temporal distribution at the mid cross-section of the groove (Movie S5) (Fig. 2). Three functional types were observed: 1) single inward vane, moving parallel to the groove floor, 2) single outward vane, moving in a 3D motion, and 3) double vanes. Irrespective, the vane(s) project more-or-less perpendicularly to the primary plane of beating.

1. Single inward vane (*J. libera* and *R. americana*)

The posterior flagellum of *J. libera* and *R. americana* remains inside the groove throughout the beat cycle. It beats in an oblique plane between the two walls: from the top of the left-side wall toward the bottom of the right-side wall (Movie S5) (Fig. 2 *A* and *B*). The

Table 1. Beat frequencies of flagella in feeding (attached) and free-swimming flagellates, swimming speeds, and estimated potential clearance rates

	Flagella beat frequencies (Hz), mean ± SD (n)				Swimming speed			
	Feeding		Free-swimming		Mean ± SD (n)	Feeding groove		
	Posterior flagellum	Anterior flagellum	Posterior flagellum	Anterior flagellum	Speed, μm s^{-1}	Flow speed, μm s^{-1}	Potential clearance rate, μm^3 s^{-1}	Specific potential clearance rate, d^{-1}
Jakoba libera	37 ± 3 (6)	–	30 ± 4 (3)	17 ± 2 (3)	14 ± 2 (3)	0.18 ± 0.05	918	3.3×10^6
Reclimonas americana	49 ± 4 (5)	48 ± 4 (5)	60 ± 5 (10)	44 ± 3 (11)	105 ± 12 (8)	0.12 ± 0.03	1,152	1.7×10^6
Kipferlia bialata	26 ± 3 (4)	6 ± 2 (5)	25 ± 14 (3)	9 ± 2 (3)	13 ± 4 (3)	0.05 ± 0.03	280	0.24×10^6
Carpediemonas membranifera	27 ± 2 (5)	6 ± 0 (5)	31 ± 3 (3)	7 ± 1 (3)	26 ± 9 (3)	0.13 ± 0.05	413	1.3×10^6
Malawimonas californiensis	42 ± 6 (5)	7 ± 1 (5)	–	–	–	–	–	–

Averages are given with SD. Number of observations in parentheses. The specific rates are normalized by cell volume.

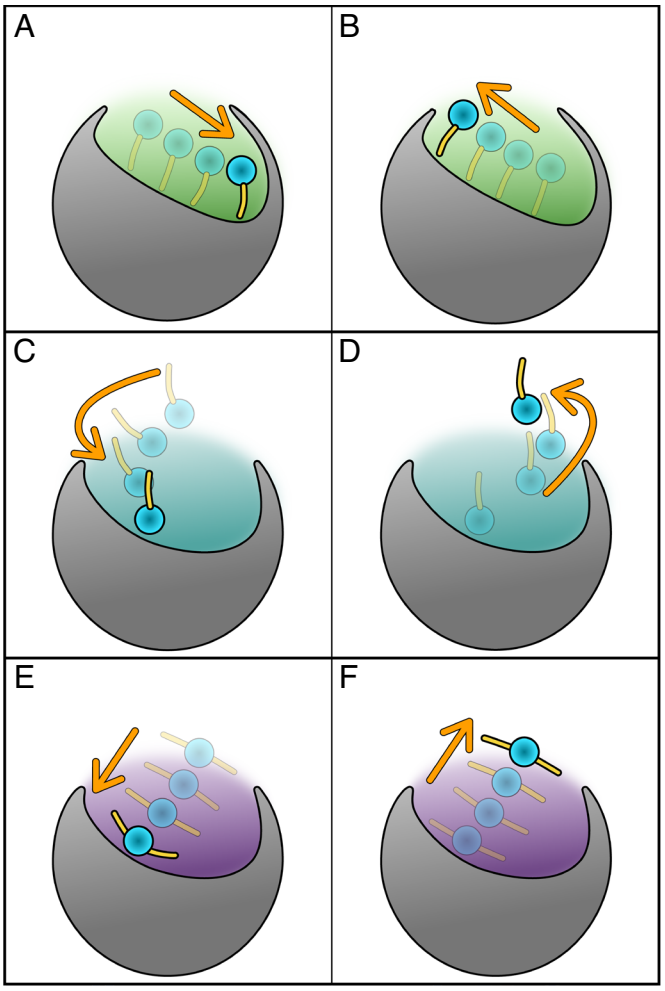

Fig. 2. Three modes of posterior flagellum kinematics inside the ventral groove. Schematic representations of mid-transversal cross-section views of the ventral groove (green, teal, and purple shadows) and the position of the flagellum (blue circle) equipped with a vane/s (yellow) between the first half of a beat cycle (panels on the *Left*) and the second half of the cycle (panels on the *Right*). The orange arrows indicate the direction of the moving flagellum. The right-side wall of the cell is on the right-side of the viewer. The cross-sections correspond to the observations of (*A* and *B*) *J. libera* and *R. americana*, (*C* and *D*) *K. bialata*; (*E* and *F*) *C. membranifera*, and *M. californiensis*. See animations in Movie S5.

taller right wall curves over the groove. The flagellar beating plane is parallel to the groove floor and the vane is sweeping across it, in proximity or in direct contact.

2. Single outward vane (*K.* bialata)

The flagellum has a terminal row of tape-like hairs (28). The beating pattern is three-dimensional, spanning from the bottom to outside of the groove (Movie S5) (Fig. 2 *C* and *D*). The initial left-side tilt of the vane becomes almost parallel to the groove floor when it collides with the base of the left wall, and it subsequently points outward when it emerges outside of the groove again at the end of the beat cycle.

3. Double vanes (*C. membranifera* and *M. californiensis*)

The outward vane has a slight tilt to the left while, symmetrically, the inward vane points to the right. The beat wave oscillates from just outside of the groove to the bottom-left corner of the cavity, executing an oblique trajectory between the walls (Movie S5) (Fig. 2 *E* and *F*). A third, much shorter vane, orthogonal to the two main vanes, has been reported for *C. membranifera* by electron microscopy (18).

Feeding Current. Example particle tracks for four species represent two-dimensional projections of three-dimensional flows and depend also on what angle the cell was observed (Fig. 3). Thus, the particle tracks can be used only to qualitatively describe the feeding current. The feeding current flows are similar among all species (despite *R. americana* having a lorica), with an accelerating flow arriving at the mid-to-anterior end of the ventral groove and leaving again from the mid-to-posterior end of the groove. Far from the ventral groove, particle motion is dominated by Brownian diffusion, and the feeding current only dominates particle motion within 10 to 30 μm of the cell.

Flow velocities in the ventral groove, estimated from the velocities of particles in the groove, varied between species by a factor of ca. 3, apparently unrelated to the beat frequency of the posterior flagellum (Table 1). All prey that enters the groove are potentially captured, therefore the volume flow rate of water through the groove is an estimate of the potential maximum clearance rate. We estimated this rate as the product of flow velocity and the cross-sectional area of the groove (*SI Appendix*, Table S1) The resulting estimates of cell-volume-specific clearance rates vary by an order of magnitude, between 0.2 to 3 × 10^6 per day (Table 1).

CFD. We developed a CFD model of a simplified generic excavate flagellate (*SI Appendix*, Fig. S2) with basic morphology and kinematics inspired by *J. libera* (*SI Appendix*, Table S1); that is, a cell with a posterior flagellum beating inside and parallel to

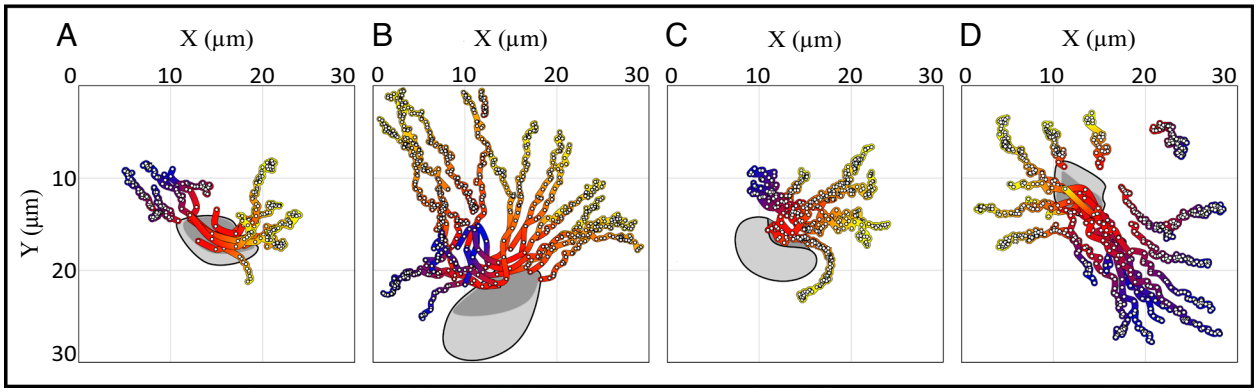

Fig. 3. Example particle tracks for 4 species: (*A*) *J. libera*, (*B*) *R. americana,* (*C*) *K. bialata,* and (*D*) *C. membranifera,*. Tracer particles are positioned (dots) at a frequency of 60 Hz (Except *R. americana*: 50 Hz), and the distance between positions thus indicates flow speed. Far from the flagellate, particle tracks are dominated by Brownian motion. The color indicates the direction of the flow, from yellow through red to blue.

the bottom of the ventral groove and equipped with an inward-oriented vane. This basic case was then modified to have other vane arrangements (outward-oriented, broader vane, two vanes), beat orientation (perpendicular to the bottom of the groove), a higher wall on the right than on the left-side of the groove (*SI Appendix*, Fig. S3), attachment to a surface positioned on the dorsal or ventral side of the cell, an anterior flagellum beating in a 3-dimensional pattern, and/or a posterior flagellum that is also active outside the ventral groove, as found in the different species described above. We varied one parameter at a time to examine the functional significance of the different morphological features. Finally, to examine the effect of having the posterior flagellum constrained in a groove, we ran a case without any groove and the flagellum instead beating above the surface of the cell (*SI Appendix*, Fig. S4). As diagnostic output characteristics we computed flow fields, power consumption, and magnitudes of the clearance rate.

The main outcomes of the CFD modeling are first that the magnitude of the clearance rate depends mainly on the beating of the posterior flagellum inside/over the ventral groove and on the dimensions of the vane, and that all other morphological features, as well as the action of the anterior flagellum, have only limited effect (Fig. 4). The model flagellates have volume flow rates through the groove of 250 to 450 $\mu m^3 s^{-1}$, of similar order to that estimated experimentally for the examined species (Fig. 4). Whether the posterior flagellum beats parallel or perpendicular to the bottom of the groove has limited effect, so both orientations observed appear equally well suited for feeding. Broader vanes lead to higher power consumption but also to higher clearance rates.

Second, the presence of the anterior flagellum and the "free" part of the posterior flagellum extending outside the groove improves the architecture of feeding current by extending the region around the cell within which the advective feeding current is strong enough to overcome the diffusive Brownian motion of passive prey particles. This is illustrated by longer streamlines that are plotted only where the Peclet number (Pe) exceeds 1 (Fig. 4); The Peclet number indicates the relative significance of advection over diffusion, Pe = au/D, where a is prey radius (0.5 μm), D is Brownian diffusion computed from Einstein relation, and u is the feeding current velocity). This enhancement of the feeding current is also visible in our observations (Fig. 3) and is most significant for flagellates attached to a surface (Fig. 4). However, the effect is modest as judged from the magnitude of the Peclet number and it happens at the cost of a substantially higher power consumption. When preying on motile bacteria that have effective diffusivities by far exceeding Brownian motion, the effect vanishes.

Finally, the containment of the vaned flagellum in the ventral groove improves the magnitude of volume flow rate through the groove. A vaned flagellum beating outside a groove creates a feeding current characterized by intense sideways oscillations that cancel out during a complete beat cycle, resulting in a lower (averaged) volume flow rate. Conversely, the presence of a groove generates a smoother and more directional flow, leading to a higher volume flow rate (Fig. 5). The advantage of beating inside a groove vanishes for a naked flagellum without a vane (Fig. 5*C*).

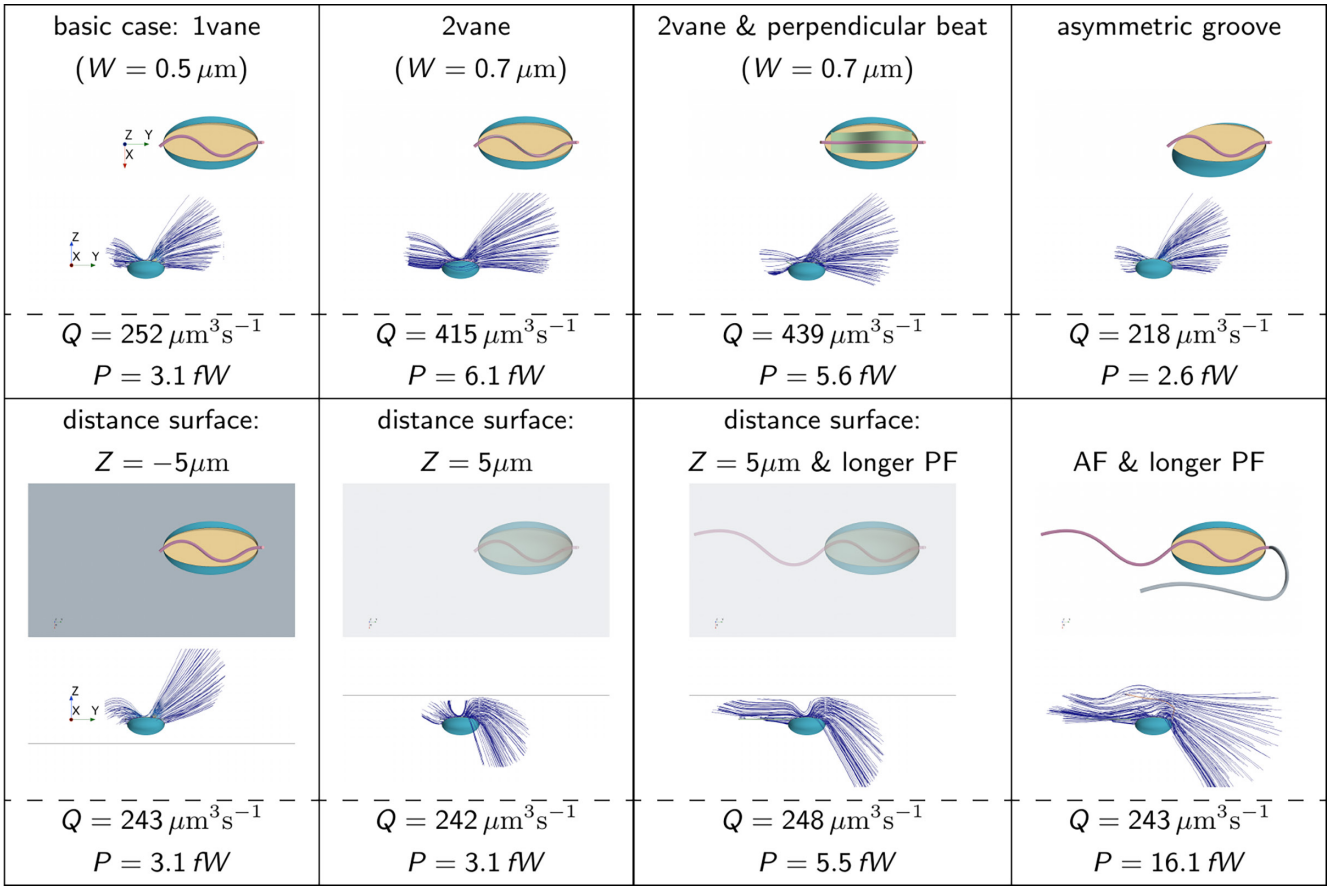

Fig. 4. CFD cases demonstrating the influence of various morphological aspects and surface proximity. In each panel, the case is first described (number of vanes, width of vane, asymmetry of groove, the presence of a surface dorsally (−5 μm) or ventrally (+5 μm) to the cell, and the presence of an active anterior and extended posterior flagellum). The anterior end of the cell is to the *Right*. Streamlines represent the averaged flow field, with sections omitted where flow velocity is below 2 μm s^{-1} (corresponding to a Peclet number of ~1 for 0.5 μm passive prey particles). This threshold indicates where the advective feeding current overcomes the diffusive Brownian motion of passive prey particles. Q is the estimated clearance rate and P the estimated power consumption.

Discussion

We have here described the suspension feeding and swimming behavior of several species of typical excavates drawn from across the three main phylogenetic groups. Our descriptions supplement earlier scattered and anecdotal observations, but the most important advance of our work is the provision of a mechanistic (physical) understanding of the functional significance of distinct morphological features and behaviors and identification of the separate roles of the two flagella. While phylogenetically diverse, the species examined are all characterized by a vaned flagellum beating in association with a ventral groove. This flagellar arrangement is primarily an adaptation to feeding, not swimming. In fact, like many other phagotrophic flagellates, excavates seem to be mainly attached to a surface when feeding, and free-swimming excavate cells appear to be slow and inefficient swimmers (Table 1). One exception is the swarmer stage of *R. americana* that lacks the flagellar vane (27) and adopts a different flagellar beat pattern than the attached foraging stage. Also, the swimming form of the jakobid *Stygiella incarcerata* usually lacks a ventral groove and has a longer anterior flagellum (29). This contrasts with the less effective swimming behavior of the "normal grooved" cells of *J. libera* described here.

The volume flow rate of water through the groove estimated here, both from particle tracking and CFD, are of similar order of magnitude as direct clearance rate estimates for *J. libera* derived from incubation experiments (30, 31), ~250 to 800 $\mu m^3\ s^{-1}$ (cf. Table 1 and Fig. 4 for our experimental and computational estimates). These estimates, in turn, are within the typical range for phagotrophic flagellates of similar sizes (4).

Key to the functioning of the flagellum in clearing prey from ambient water is the interaction between the groove and the vaned flagellum. A vaned flagellum beating in a depression on the cell surface may be particularly efficient in generating a feeding current: First, having the force near the cell brings the feeding current streamlines near to the cell surface (Figs. 3 and 4) where prey is captured, thus increasing prey encounter and retention rates. Second, adding a vane to a flagellum is an energy-efficient way of increasing the clearance rate, compared to increasing the beat frequency. The power consumption of a beating flagellum constrained in a groove increases linearly with the width of the flagellum, as does the resulting clearance rate, and the relation between the two is therefore near-linear (Fig. 5*C*). In contrast, because in the viscous environment in which flagellates operate the clearance rate scales with the beat frequency while the power consumption with the beat frequency squared, the clearance rate increases only with the square root of the power consumption (Fig. 5*C*), rendering this a much less energy-efficient way of increasing the clearance rate. One may question the significance of the energy-efficiency argument, because the operational cost of flagella typically constitutes only a tiny fraction of total metabolism of rapidly growing cells (32). However, flagellates may increase their activity but reduce their metabolism by orders of magnitude when resources are scarce (33)—a state in which they may be much of the time in nature—and in this situation, the energy-efficiency of feeding may become important.

Vaned constrained flagella are widespread among phagotrophic flagellates. Choanoflagellates have a vaned flagellum beating inside a collar filter, and the equatorial flagellum of dinoflagellates drives a diaphragm-like sock in the circumferential depression on the cell surface (cingulum), arrangements that both allow efficient feeding currents (9). These are not homologous structures, however. For example, the vanes in excavates are each supported by intraflagellar paraxonemal lamella, while the fibrillar vanes of choanoflagellates extend out of the flagellar membrane, and the cingulum-contained flagellum in dinoflagellates is equivalent to the anterior flagellum of excavates, rather than their posterior flagellum.

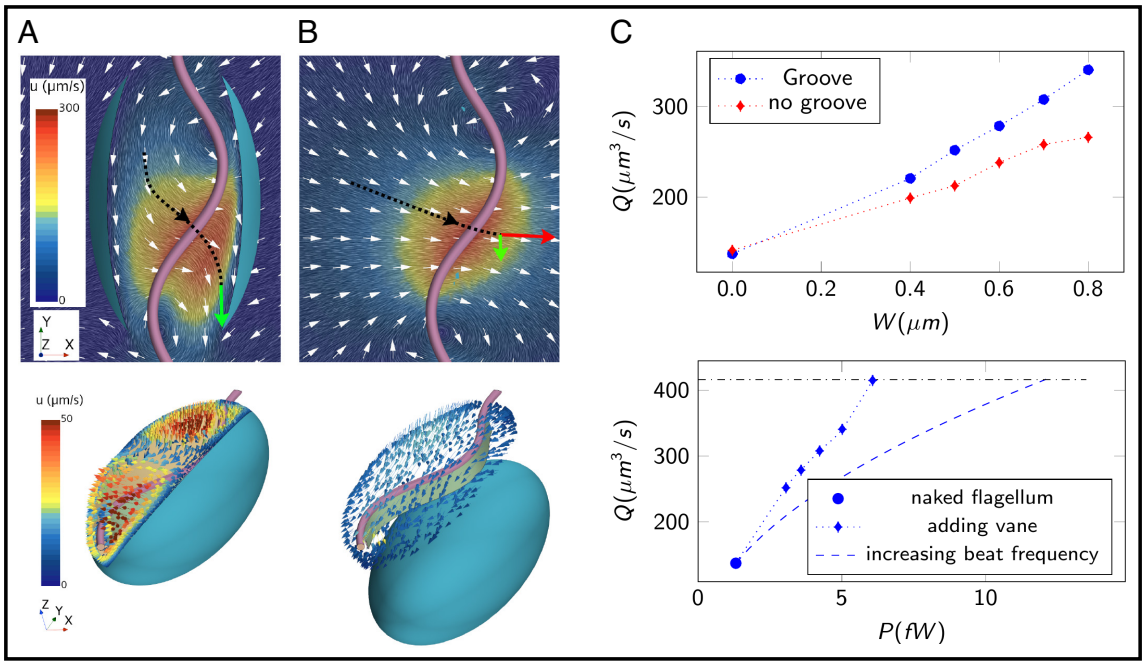

Fig. 5. Effect of confinement on the feeding current generated by a (vaned) flagellum. A snapshot of the flow during the flagellum beating cycle (*A*, *Top*) shows that the vaned flagellum pushes the flow against the wall of the groove, directing the flow posteriorly (green arrow). This interaction, during the complete beat cycle, results in a relatively strong averaged flow through the groove (*A*, *Bottom*). In the absence of the groove (*B*, *Top*), the vaned flagellum pushes the flow in free space where only a small component of such flow is directed downward (green arrow), while most of the flow is directed sideways (red arrow). The oscillating sideways flows cancel out during the beat cycle, resulting in a weak average flow (*B*, *Bottom*). The clearance rate (*Q*) increases with the width of the vane (*W*), but most so for a flagellum within a groove (*C*, *Top*). Clearance rate (*Q*) vs. power consumption (P) (*C*, *Bottom*). Comparing clearance rates when adding vanes versus increasing the beat frequency. The data points represent simulation results for vane widths of 0.4 μm, 0.5 μm, 0.7 μm, 0.8 μm (1-vane configuration), and the last point 0.7μm (2-vane configuration). The dashed line illustrates the effect of increasing the beat frequency given by $Q = Q_{naked} * \sqrt{P/P_{naked}}$.

Conversely, there are poorly studied phagotrophic flagellates from other deep branches of the eukaryotic tree of life with a flagellar arrangement similar and potentially homologous to that found in the typical excavates, namely a posterior flagellum with a vane supported by an intraflagellar lamellum that beats in association with a conspicuous ventral groove. The best examples are colponemids within the alveolates (34, 35) and the Nebulidia within the newest proposed supergroup—Provora (24, 36). The foraging mechanisms in these species are yet to be explored in detail, but the similarity of structures may suggest similar fluid dynamic behavior, albeit both colponemids and nebulids are eukaryovores and ingest their prey at the anterior end of the cell, not the posterior (35).

The anterior flagellum and the free part of the posterior flagellum apparently do not directly contribute to driving water through the groove. However, they may mix the ambient water and increase the spatial extension where the feeding current is effective, thus constantly providing fresh, prey-containing water to the immediate vicinity of the cell. Such mixing may be relevant for cells attached to a surface where the viscous boundary layer may rapidly be depleted of prey. Typical excavates attached to a marine snow particle may not only be feeding on the elevated concentration of bacteria swarming around a particle (37) but may also be feeding on the high density of bacteria typically attached to the particle surface (38), as observed above for *C. membranifera*. Here again, the interaction between the posterior flagellum and the groove appears important.

Phylogenetic Implications of Functional Morphology. In this study, we examined species from all three principal clades of "excavates"—Discoba, Metamonada, and Malawimonadida. The foraging mechanisms appear fundamentally similar across the examined species, in terms of posterior flagellum activity, feeding current magnitude, and engulfment behavior. Arguably, the greatest differences, between *Kipferlia* and the other subjects, divide species within a principal clade rather than between them, since *Kipferlia* and *Carpediemonas* are both metamonads. This functional similarity is broadly consonant with the hypothesis that the typical excavate cell architecture is ultimately homologous across Discoba, Metamonada, and Malawimonadida (7, 15, 39). The relationships among excavates are not well resolved, however, and most recent phylogenomic analyses show the three main clades representing at least two very distantly related lineages (5, 7, 24, 40). Reconciling the excavate homology hypothesis with these molecular phylogenetic results suggests that the LECA was a typical excavate in its morphology. Indeed, some form of excavate ancestry for all living eukaryotes has been advocated after some "rooted" phylogenomic analyses of eukaryotes (6, 8). It is a credible hypothesis, therefore, that the typical excavate foraging system characterized here may have been used by our distant ancestors more than 1 billion years ago (41). This suggests an ancient history of bacterivory via relatively elaborate suspension feeding (rather than feeding solely by creeping on surfaces, for example) and permits reasonable estimates of the effectiveness of that feeding within ancient microbial ecosystems. Given these biological and earth ecosystem evolution stakes, more research into the details of typical excavate cell architecture, their extant diversity, and their phylogenetic relationships, is warranted.

Material and Methods

Culturing. The flagellates were maintained in the Simpson Lab, Dalhousie University (*C. membranifera*), or kindly provided by Franz Lang, Université de Montréal (*R. americana*, *J. libera*, "*M. californiensis*") or Julie Boisard and Courtney Stairs, University of Lund (*K. bialata*); see *SI Appendix*, Table S2 for isolate ID and Genbank Accession numbers. Cultures were maintained in the dark at 18 °C in highly diluted Luria Broth medium (Miller's formulation) to feed the naturally occurring bacteria that served as prey. The aerobic freshwater species, *R. americana*, grew with 0.3% LB in Milli-Q® water; the aerobic marine species *J. libera* and *M. californiensis* grew with 0.3% LB in filtered and pasteurized North Sea water (salinity 30‰); and the anaerobic marine species *C. membranifera* and *K. bialata* grew in 3% LB in sterilized North Sea water under near-anoxia established by the prokaryotic growth on this richer medium.

Microscope Imaging. Phase contrast imaging was performed with an Olympus IX71 inverted microscope equipped with an Olympus UPLanFL N oil immersion ×100/1.30 objective and an attached high-speed *Phantom Camera* (Miro LAB 320). Videos had a minimum resolution of 512 × 512 pixels and were recorded at 300 or 500 frames per second. The effects of light heating were mitigated with short exposure intervals (<10 min) at moderate intensities during recordings. Videos and images were analyzed using open-source software ImageJ (Fiji).

Aerobic flagellate species were observed by mounting 100 µL of culture between two glass coverslips (24 × 24 mm) that were spaced by small blobs of Vaseline® in each corner. The observation chamber for anaerobic species consisted of a plastic ring (16 mm inner diameter and 1.5 mm height) fixed with Vaseline® to a coverslip, filled with 300 µL of culture, and then sealed on top with a second coverslip. The latter ring chamber setup was also used for all species when visualizing their flow fields with tracer particles (see below).

Morphometrics. Morphometrics and cross-sectional areas of the groove were estimated from live images of feeding cells extracted from videos (*SI Appendix*, Fig. S1 *B–D*), assisted by TEM images from the literature (16, 18, 42) *SI Appendix*, Table S1). Volumes of individual flagellate cells were estimated using a Coulter Counter.

Flow Fields. The ring chamber was filled with a dilute suspension of flagellates, and a single cell was focused under the microscope. Then, tracer particles (0.5 ± 0.015 µm latex beads) were gently added to the chamber sealed with a coverslip. Videos of each of four species (*J. libera*, *R. americana*, *K. bialata*, and *C. membranifera*) were selected for analyses, and particles were tracked at a frequency of 50 or 60 Hz using the Manual Tracking function in ImageJ.

Potential Clearance Rates. Potential clearance rates were estimated as the volume flow rate through the groove on the assumption that particles transported into the ventral groove can all be considered captured. We selected specimens with the ventral groove oriented in the focal plane to estimate the velocity of particles in the groove, and the volume flow rate was then estimated by multiplying the average particle velocity with the cross-sectional area of the groove.

CFD. CFD modeling allows one to quantify the flow field generated by a beating flagellum, given known morphology, wave patterns, and beat kinematics, by numerically solving the flow-governing Navier–Stokes equations. The technical details are described in *SI Appendix*.

Data, Materials, and Software Availability. All original code used in this study is available at DTU data DTU Data at https://doi.org/10.11583/DTU.25663326.v1 (43). All data are available in the paper or in supporting information.

ACKNOWLEDGMENTS. Portions of the paper were developed from the thesis of S.S. Fredrik Ryderheim helped with Fig. 1, and Andrea Salvia Punsoda helped with experiments. We received funding from The Independent Research Fund Denmark (7014-00033B), the Carlsberg Foundation (CF17-0495), the Simons Foundation (931976), and the European Union's Horizon 2020 research and innovation programme under Marie Skłodowska-Curie grant agreement no. 955910. The Centre for Ocean Life is supported by the Villum Foundation.

Author affiliations: [a]Centre for Ocean Life, National Institute of Aquatic Resources, Technical University of Denmark, Kgs Lyngby 2800, Denmark; and [b]Department of Biology, Centre for Comparative Genomics and Evolutionary Bioinformatics, Dalhousie University, Halifax NS B3H 4R2, Canada

1. T. Fenchel, Ecology of heterotrophic microflagellates. IV quantitative occurrence and importance as bacterial consumers. *Mar. Ecol. Prog. Ser.* **9**, 35–42 (1982).
2. D. V. Tikhonenkov, Predatory flagellates–The new recently discovered deep branches of the eukaryotic tree and their evolutionary and ecological significance. *Protistology* **14**, 15–22 (2020).
3. T. Kiørboe, Fluid dynamic constraints on resource acquisition in small pelagic organisms. *Eur. Phys. J. Spec. Top* **225**, 669–683 (2016).
4. K. F. Edwards, Q. Li, G. F. Steward, Ingestion kinetics of mixotrophic and heterotrophic flagellates. *Limnol. Oceanogr.* **68**, 917–927 (2023).
5. Y. Eglit *et al.*, Meteora sporadica, a protist with incredible cell architecture, is related to Hemimastigophora. *Curr. Biol.* **34**, 451–459.e6 (2024).
6. R. Derelle *et al.*, Bacterial proteins pinpoint a single eukaryotic root. *Proc. Natl. Acad. Sci. U.S.A.* **112**, E693–E699 (2015).
7. A. A. Heiss *et al.*, Combined morphological and phylogenomic re-examination of malawimonads, a critical taxon for inferring the evolutionary history of eukaryotes. *R. Soc. Open Sci.* **5**, 171707 (2018).
8. C. Al Jewari, S. L. Baldauf, An excavate root for the eukaryote tree of life. *Sci. Adv.* **9**, eade4973 (2023).
9. T. Kiørboe, Predation in a microbial World: Mechanisms and trade-offs of flagellate foraging. *Ann. Rev. Mar. Sci.* **16**, 361–381 (2024).
10. S. Suzuki-Tellier, A. Andersen, T. Kiørboe, Mechanisms and fluid dynamics of foraging in heterotrophic nanoflagellates. *Limnol. Oceanogr.* **67**, 1287–1298 (2022).
11. S. S. Asadzadeh, J. H. Walther, A. Andersen, T. Kiørboe, S. S. Asadzadeh, Hydrodynamic interactions are key in thrust-generation of hairy flagella. *Phys. Rev. Fluids* **7**, 073101 (2022).
12. J. M. Pinskey *et al.*, Three-dimensional flagella structures from animals' closest unicellular relatives, the Choanoflagellates. *Elife* **11**, e78133 (2022).
13. L. T. Nielsen *et al.*, Hydrodynamics of microbial filter feeding. *Proc. Natl. Acad. Sci. U.S.A.* **114**, 9373–9378 (2017).
14. J. T. Berdach, In situ preservation of the transverse flagellum of Peridinium cinctum (dinophyceae) for scanning microscopy. *J. Phycol.* **13**, 243–251 (1977).
15. A. G. B. Simpson, Cytoskeletal organization, phylogenetic affinities and systematics in the contentious taxon Excavata (Eukaryota). *Int. J. Syst. Evol. Microbiol.* **53**, 1759–1777 (2003).
16. D. J. Patterson, Jakoba Libera (Ruinen, 1938), A Heterotrophic flagellate from deep oceanic sediments. *J. Marine Biol. Assoc. U. K.* **70**, 381–393 (1990).
17. M. Flavin, T. A. Nerad, Reclinomonas americana N. G., N., Sp., a New freshwater heterotrophic flagellate. *J. Eukaryotic Microbiol.* **40**, 172–179 (1993).
18. A. G. B. Simpson, D. J. Patterson, The ultrastructure of Carpediemonas membranifera (Eukaryota) with reference to the "Excavate Hypothesis". *Europ. J. Protistol.* **35**, 353–370 (1999).
19. E. Lara, A. Chatzinotas, A. G. B. Simpson, Andalucia (n. Gen.)–The deepest branch within jakobids (Jakobida; Excavata), based on morphological and molecular study of a new flagellate from soil. *J. Eukaryotic Microbiol.* **53**, 112–120 (2006).
20. T. Pánek *et al.*, Combined culture-based and culture-independent approaches provide insights into diversity of jakobids, an extremely plesiomorphic eukaryotic lineage. *Front. Microbiol.* **6**, 1288 (2015).
21. A. Stock, K. Jurgens, J. Bunge, T. Stoeck, Protistan diversity in suboxic and anoxic waters of the Gotland Deep (Baltic Sea) as revealed by 18SrRNA clone libraries. *Aquatic Microbial. Ecol.* **55**, 267–284 (2009).
22. S. Suzuki-Tellier, T. Kiørboe, A. G. B. Simpson, The function of the feeding groove of 'typical excavate' flagellates. *J. Eukaryotic Microbiol.* **71**, e13016 (2024).
23. A. Yabuki, Y. Gyaltshen, A. A. Heiss, K. Fujikura, E. Kim, Ophirina amphinema n. gen., n. sp., a new deeply branching discobid with phylogenetic affinity to jakobids. *Sci. Rep.* **8**, 16219 (2018).
24. D. V. Tikhonenkov *et al.*, Microbial predators form a new supergroup of eukaryotes. *Nature* **612**, 714–719 (2022).
25. D. He, O. Fiz-Palacios, C. J. Fu, C. C. Tsai, S. L. Baldauf, An alternative root for the eukaryote tree of life. *Curr. Biol.* **24**, 465–470 (2014).
26. B. S. Leander, Eukaryotic evolution: Deep phylogeny does not imply morphological novelty. *Curr. Biol.* **33**, R112–R114 (2023).
27. C. J. O'kelly, Ultrastructure of trophozoites, zoospores and cysts of reclinomonas americana Flavin & Nerad, 1993 {Protista incertae sedis: Histionidae}. *Eur. J. Protitol.* **33**, 337–348 (1997).
28. N. Yubuki, A. G. B. Simpson, B. S. Leander, Comprehensive ultrastructure of Kipferlia bialata provides evidence for character evolution within the Fornicata (Excavata). *Protist* **164**, 423–439 (2013).
29. A. G. B. Simpson, D. J. Patterson, On core jakobids and excavate taxa: The ultrastructure of Jakoba incarcerata. *J. Eukaryotic Microbiol.* **48**, 480–492 (2001).
30. J. D. Eccleston-Parry, B. S. C. Leadbeater, A comparison of the growth kinetics of six marine heterotrophic nanoflagellates fed with one bacterial species. *Mar. Ecol. Prog. Ser.* **105**, 167–177 (1994).
31. B. R. Mohapatra, K. Fukami, Effect of different bacterial species on the growth kinetics of the heterotrophic nanoflagellate Jakoba libera. *Basic Appl. Ecol.* **6**, 67–73 (2005).
32. P. E. Schavemaker, M. Lynch, Flagellar energy costs across the tree of life. *Elife* **11**, e77266 (2022).
33. T. Fenchel, "Adaptations to a feast and famine existence in protozoa" in *Energy Transformation in Cells and Organisms*, W. Wieser, E. Gnerider, Eds. (Thieme, 1989), pp. 290–295.
34. J. Janouškovec *et al.*, Colponemids represent multiple ancient alveolate lineages. *Curr. Biol.* **23**, 2546–2552 (2013).
35. A. S. Gigeroff, Y. Eglit, A. G. B. Simpson, Characterisation and cultivation of new lineages of colponemids, a critical assemblage for inferring alveolate evolution. *Protist* **174**, 125949 (2023), 10.1016/j.protis.2023.125949.
36. J. Janouškovec *et al.*, A new lineage of eukaryotes illuminates early mitochondrial genome reduction. *Curr. Biol.* **27**, 3717–3724.e5 (2017).
37. R. Stocker, J. R. Seymour, Ecology and physics of bacterial chemotaxis in the ocean. *Microbiol. Mol. Biol. Rev* **76**, 792–812 (2012).
38. T. Kiørboe, H. P. Grossart, H. Ploug, K. Tang, B. Auer, Particle-associated flagellates: Swimming patterns, colonization rates, and grazing on attached bacteria. *Aquatic Microbial. Ecol.* **35**, 141–152 (2004).
39. C. J. O'Kelly, The jakobid flagellates: Structural features of jakoba, reclinomonas and histiona and implications for the early diversification of eukaryotes. *J. Eukaryotic Microbiol.* **40**, 627–636 (1993).
40. E. Yazaki *et al.*, The closest lineage of Archaeplastida is revealed by phylogenomics analyses that include Microheliella maris. *Open Biol.* **12**, 210376 (2022).
41. S. M. Porter, Insights into eukaryogenesis from the fossil record. *Interface Focus* **10**, 20190105 (2020).
42. M. Kolisko *et al.*, A wide diversity of previously undetected free-living relatives of diplomonads isolated from marine/saline habitats. *Environ. Microbiol.* **12**, 2700–2710 (2010).
43. T. Kiørboe, S. S. Asadzadeh, Excavate_codes. Technical University of Denmark. Software. https://doi.org/10.11583/DTU.25663326. Deposited 22 April 2024.